A Presynaptic Regulatory System Acts Transsynaptically via Mon1 to Regulate Glutamate Receptor Levels in *Drosophila*

Senthilkumar Deivasigamani,*[,1] Anagha Basargekar,[†,1] Kumari Shweta,[†] Pooja Sonavane,[†,2] Girish S. Ratnaparkhi,*[,3] and Anuradha Ratnaparkhi[†,3]

*Indian Institute of Science Education and Research, Pashan, Pune 411 008, India, and [†]Agharkar Research Institute, Pune 411 004, India

ABSTRACT Mon1 is an evolutionarily conserved protein involved in the conversion of Rab5 positive early endosomes to late endosomes through the recruitment of Rab7. We have identified a role for *Drosophila* Mon1 in regulating glutamate receptor levels at the larval neuromuscular junction. We generated mutants in *Dmon1* through *P*-element excision. These mutants are short-lived with strong motor defects. At the synapse, the mutants show altered bouton morphology with several small supernumerary or satellite boutons surrounding a mature bouton; a significant increase in expression of GluRIIA and reduced expression of Bruchpilot. Neuronal knockdown of *Dmon1* is sufficient to increase GluRIIA levels, suggesting its involvement in a presynaptic mechanism that regulates postsynaptic receptor levels. Ultrastructural analysis of mutant synapses reveals significantly smaller synaptic vesicles. Overexpression of *vglut* suppresses the defects in synaptic morphology and also downregulates GluRIIA levels in *Dmon1* mutants, suggesting that homeostatic mechanisms are not affected in these mutants. We propose that DMon1 is part of a presynaptically regulated trans-synaptic mechanism that regulates GluRIIA levels at the larval neuromuscular junction.

KEYWORDS *Drosophila*; Rabs; Mon1; synapse; GluRIIA

SYNAPTIC strength is tightly modulated through expression of presynaptic and postsynaptic proteins. The regulation occurs at the level of transcription, translation, or degradation via the ubiquitin–proteosome and lysosomal pathways (DiAntonio *et al.* 2001; Dobie and Craig 2007; Fernandez-Monreal *et al.* 2012). The larval neuromuscular junction (NMJ) in *Drosophila* is glutamatergic and serves as an excellent system to study regulation of receptor levels—one of the key factors underlying synaptic strength and functional plasticity.

During development, expression of the glutamate receptor subunits, including GluRIIA, is regulated by Lola—a BTB Zn-finger domain transcription factor in an activity-dependent manner (Fukui *et al.* 2012). The abundance of the receptor at the synapse is sensitive to presynaptic inputs and is subject to translational control by RNA binding proteins and microRNAs (Sigrist *et al.* 2000, 2003; Menon *et al.* 2004; Heckscher *et al.* 2007; Karr *et al.* 2009; Menon *et al.* 2009). The precise mechanism that controls this regulation is not clear. In addition, the role of endocytic pathways in regulating glutamate receptor levels through trafficking to and from the synapse, as well as the molecular pathways governing protein turnover are still poorly understood.

Endocytic vesicles carrying cell surface proteins such as signaling molecules, cellular organelles, and engulfed pathogens sort their cargo such that they are either recycled or targeted to the lysosome for degradation. The trafficking of these vesicles, through fusion with appropriate membrane compartments, is regulated by Rab GTPases—a family of small G-proteins. Mon1 was first identified in yeast as a protein, which in complex with CCZ1, regulates all fusion events to the lysosome (Wang *et al.* 2002, 2003). Subsequent studies in *Caenorhabditis elegans* identified SAND-1/Mon1 as an

doi: 10.1534/genetics.115.177402
Manuscript received April 16, 2015; accepted for publication August 10, 2015; published Early Online August 19, 2015.
Supporting information is available online at www.genetics.org/lookup/suppl/doi:10.1534/genetics.115.177402/-/DC1.
[1]These authors contributed equally to this work.
[2]Present address: Department of Cell Biology, University of Virginia, Charlottesville, VA 22908.
[3]Corresponding authors: Agharkar Research Institute, Developmental Biology group, G.G. Agarkar Rd., Pune 411 004, India. E-mail: anu.aripune@gmail.com; and Indian Institute of Science Education and Research, Pashan, Pune 411 008, India. E-mail: girish@iiserpune.ac.in

effector of Rab5, and as a factor essential for recruitment of Rab7, highlighting its role in the conversion of Rab5 positive early endosome to Rab7 containing late endosome (Poteryaev *et al.* 2007; Kinchen and Ravichandran 2010; Poteryaev *et al.* 2010). Consistent with these studies, loss of Mon1 in *Drosophila* is shown to result in enlarged endosomes and loss of endosomal Rab7, implying a role for DMon1 in the recruitment of Rab7 (Yousefian *et al.* 2013).

We are interested in pathways that regulate synaptic function for their implication in motor neuron disease (Ratnaparkhi *et al.* 2008). We isolated a mutation in *Mon1* while screening for *P*-element excisions in the neighboring gene *pog*. A striking phenotype observed in these mutants was their inability to walk or climb normally. The presence of a strong motor defect implied impaired neuronal or muscle dysfunction that prompted us to examine these mutants in greater detail.

In this study, we describe a role for *Drosophila Mon1* (*Dmon1*) in regulating GluRIIA expression at the NMJ. *Dmon1* mutants show multiple synaptic phenotypes. A striking phenotype among these is the huge increase in postsynaptic GluRIIA levels. The increase in receptor levels appears to be posttranscriptional, suggestive of control at the level or translation, trafficking, or protein degradation. We show that neuronal knockdown of *Dmon1* is sufficient to phenocopy the GluRIIA phenotype, indicating the involvement of a presynaptic mechanism in regulating receptor levels. We find that *Dmon1* mutants have smaller neurotransmitter vesicles, and overexpression of the vesicular glutamate transporter (*vglut*) suppresses the synaptic morphology and GluRIIA phenotype in *Dmon1* mutants. Our results thus suggest a novel role for DMon1 in regulating GluRIIA levels, which we hypothesize may, in part, be via a mechanism linked to neurotransmitter release.

Materials and Methods

Generation and mapping of Mon1 mutants

The mutants $Dmon1^{\Delta 181}$ and $Dmon1^{\Delta 129}$ were generated by excising the *pUAST-Rab21*::*YFP* insertion (Bloomington *Drosophila* Stock Center) using standard genetic methods. Δ181 and Δ129 failed to complement each other and deficiency lines *Df (2L) 9062*, *Df (2L) 6010*, and *Df(2L)8012*, which span the genomic locus, but showed complementation to $mRpS2^{EY10086}$ (Mathew *et al.* 2009), suggesting that the deletion does not extend to mRpS2.

Molecular mapping was carried out using PCR on genomic DNA isolated from homozygous third instar mutant larvae identified using second chromosome GFP balancers. To map the deletion, the entire region spanning genes *Dmon1* and *pog* was analyzed by PCR.

Primers 11926_2F and primer 31660_Ex2R (Figure 1A, gray arrows) amplified a 850-bp product with Δ181 (2128 bases in wild type). This was cloned and sequenced to determine the breakpoints of the deletion. In Δ129 mutants, primers 3F in CG11926 and Int1_R2 in CG31660/pog (Figure 1A, red arrows) amplified a 550-bp band instead of the expected 2.4 kb. The *pog* primer sequences used for mapping include: Ex 31660_1F, ACTGGTGCTGGCCGACCGCTC; Ex31660_2R, AACCGACAGA TACACGAGCATT; Intron1, F1AATGCTCGTGTATCTGTCGGTT; Intron1 F2, TGCCAGCATCAGGCTATCAAG; and Intron1 R2, CTTGATAGCCTGATGCTGGCA. *Dmon1* primers used for deletion mapping and RT-PCR are: 11926_1F, ATGGAAGTAGAGCA GACGTCAGT; 11926_ 2F, AGCACGACAGTCTGTGGCAGG; 11926_ 3F, ATCTGCATGCGCATGTCTCGTAC; and 11926_ 4F, GAAACCATGCCACATTCTAAGCTT. The reverse primers were complementary to forward primers. Primers used for quantitative PCR include: RP49_forward, GACGCTTCAAGGGACAGTATC; RP49_reverse, AAACGCGGTTCTGCATGAG; GluRIIA_ forward, CGCACCTTCACTCTGATCTATG; and GluRIIA_reverse, CTGTCTCCTTCCACAATATCCG.

Drosophila stocks and fly husbandry

All stocks were reared on regular corn flour medium. The following fly stocks were used: *pUAST-Rab21*::*YFP* (no. 23242), *Df(2L) 9062*, and *Df(2L)6010* were from the Bloomington Stock Center; *Dmon1* RNAi line (GD38600) was obtained from the Vienna *Drosophila* RNAi Center (VDRC); *UAS-dvglut* and *Sp/Cyo, wglacZ*; *UAS-mon1*::*HA* were kind gifts from A. DiAntonio, Washington University, and T. Klein, University of Dusseldorf, respectively. Except where stated, all experiments were carried out at 25°.

Behavioral assays

Life span assays were carried out at 25°. The flies were monitored every day and transferred to fresh medium every other day. Measurement of climbing speed was carried out as described previously for *spastin* mutants (Sherwood *et al.* 2004). Individually maintained, control and mutant flies were evaluated for climbing at 24–26 hr, 120 hr (day 5), and 192 hr (day 8) posteclosion. Each individual animal was subjected to three trials and the speed was calculated as the average of all three trials. Climbing ability was calculated by scoring for the number of flies that climbed 6 cm in 5 sec.

Immunohistochemistry and image analysis

Wandering third instar larvae were dissected in PBS and fixed with Bouins fixative (15 min). The following antibodies were used: anti-FasciclinII or mAb1D4 (1:15 or 1:25, Developmental Studies Hybridoma Bank (DSHB); mAbnc82 (1:50, DSHB); anti-GluRIIA/mAb8B4D2 (1:200, ascites; DSHB); anti-HRP (1:1000, Sigma-Aldrich); anti-Rab5 [1:200 (for Figure 5) and 1:500, AbCam]; anti-HA (1:200, Sigma, no. 9658); anti-Rab7 (1:100) (Chinchore *et al.* 2009); and anti-GluRIIB and anti-vGlut (1:2000 and 1:500, gift from A. DiAntonio and Herman Aberle respectively). For anti-GluRIIB staining, animals were fixed for 1 min in Bouins fixative. For anti-Rab5 and anti-Rab7, animals were fixed using 4% paraformaldehyde for 20 min. Confocal imaging was carried out on a Zeiss 710 imaging system at Indian Institute of Science Education and Research (IISER). All confocal images were taken using a 63× objective (N.A. = 1.4).

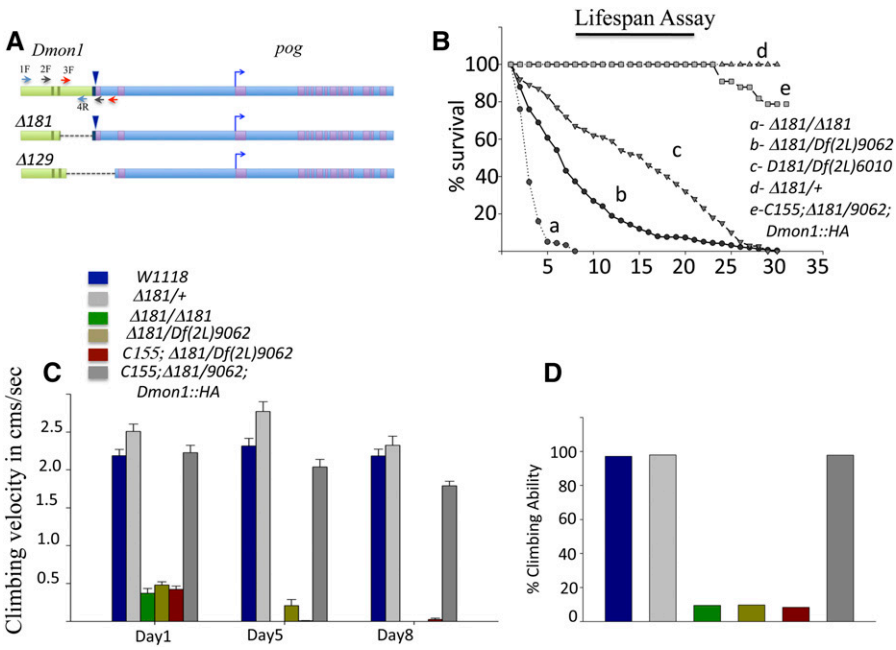

Figure 1 Characterization of *Dmon1* mutants. (A) Genomic region spanning *CG11926/Dmon1* (light green) and *CG31660/pog* (light blue). A blue arrowhead marks the site of insertion of the excised *pUASt-YFP.Rab21*. Deletions generated for line Δ181 and Δ129 are marked. (B) Lifespan defect in *Dmon1* mutants. $Dmon1^{\Delta 181}$ flies (a, n = 91) do not survive beyond 10 days while $Dmon1^{\Delta 181}/Df(2L)9062$ (b, n = 316) and $Dmon1^{\Delta 181}/Df(2L)6010$ (c, n = 259), have half-lives of ~7 and 18 days, respectively. Expression of *UAS-Dmon1::HA* in $Dmon1^{\Delta 181}/Df(2L)9062$ using *C155*-GAL4 rescues the lifespan defect in $Dmon1^{\Delta 181}/Df(2L9062)$ flies (e, n = 33) to near controls ($Dmon1^{\Delta 181}$/+, d, n = 50). (C) Climbing speed of wild type and *Dmon1* mutants. w1118 and $Dmon1^{\Delta 181}$/+ flies show comparable climbing speeds on day 1 and on day 8. $Dmon1^{\Delta 181}$, $Dmon1^{\Delta 181}/Df(2L)9062$, and *C155*; $Dmon1^{\Delta 181}/Df(2L)9062$ in contrast, are poor climbers ($P < 0.001$). Panneuronal expression of *UAS-Dmon1::HA* in $Dmon1^{\Delta 181}/Df(2L)9062$ rescues the climbing defect. Error bars represent standard error. (D) Climbing ability of w1118 and *Dmon1* mutants. W1118, $Dmon1^{\Delta 181}$/+ (97.95%) and rescue flies show robust climbing ability. Less than 10% of $Dmon1^{\Delta 181}$, $Dmon1^{\Delta 181}/Df(2L)9062$, and *C155*-GAL4; $Dmon1^{\Delta 181}/Df(2L)9062$ are able to climb.

Image analysis and fluorescence intensity measurements were carried out using ImageJ software (National Institutes of Health, NIH, Bethesda). Quantititation of GluRIIA and GluRIIB levels was carried out using the method described previously in Menon *et al.* (2009). The average gray value per synapse was determined by measuring the intensity of three individual boutons. In each case, the measured values were normalized to the background intensity for the same area. Since the mutants show significant GluRIIA staining in muscles, a region of the nucleus or regions free of GluRIIA staining was chosen for background normalization.

Analysis of the size and intensity of Brp punctae was carried out as described in Dickman *et al.* (2006). Briefly, three times the background was subtracted from the image and the resulting image was duplicated. One duplicate image was converted to binary and segmented using the watershed algorithm. Puncta size was measured from the segmented binary image using the "analyze particles" tool in ImageJ and intensity using the "redirect" option referring to the nonbinary image in the "set measurements" option. Control and experimental larvae used for quantitation were processed simultaneously for immunostaining. A master mix of the antibodies at appropriate dilutions was made prior to addition to individual tubes. Imaging was carried out under identical confocal settings. Figures were assembled using Adobe Photoshop CS4 and PowerPoint. Statistical analysis (Student's *t*-test and one-way ANOVA for Figure 4) was carried out using Sigma Plot 10. The 3D volume rendering of the bouton for Figure 7 was carried out using IMARIS software at IISER.

TEM analysis

Wild-type and mutant third instar larvae were processed for electron microscopy as described (Ratnaparkhi *et al.* 2008). Briefly, the larvae were dissected in PBS and fixed for 2 hr with 2% glutaraldehyde in 0.12 M sodium cacodylate buffer (pH 7.4). Samples were postfixed with 1% osmium tetroxide in 0.12 M sodium cacodylate with rotation. Staining with 2% uranyl acetate was carried out *en bloc* for at least 1 hr. The samples were washed, dehydrated using an ethanol series, and embedded in araldite resin. Analysis was carried out on a FEI Tecnai G2 spirit, 120 Kv transmission electron microscope. Type 1b boutons from segments A2 and A3 were imaged and used for analysis. Electron micrographs were analyzed using ImageJ. A total of 200 vesicles from 10 boutons (wild type, four animals) and 100 vesicles from 7 boutons (three animals) were used for quantitation. In most cases, vesicles near active zones were chosen for analysis.

Real-time PCR

Third instar larvae were dissected in PBS and RNA was isolated from body wall muscles of the larvae using TRIzol reagent (Invitrogen) according to the manufacturer's instructions. An equal amount of RNA from W1118 (control) and Δ181 larvae was used for cDNA synthesis. Real-time PCR was performed for *rp49* and *GluRIIA* with SYBR green mix (Kappa Biosystem) on an Eppendorf RealPlex2. The fold change was calculated using $2^{-\Delta(\Delta CT)}$.

Data availability

Supplemental information present in Figure S1, Figure S2, and Figure S3.

Results

Dmon1 mutants have lifespan and motor defects

We generated and identified a mutation in *Dmon1* through imprecise excision of pUASt-YFP::Rab21 located at the 3′ end of *Dmon1* and 5′ upstream of its neighbor *pog*. Two of the putative excision lines Δ129 and Δ181 failed to complement the deficiencies spanning the locus. Molecular mapping using PCR revealed the excision in Δ129 to span the 3′ end of *Dmon1* and 5′ end of *pog*. The deletion in Δ181 was restricted to *Dmon1*, extending from position 4851580 in the second intron to 4852858—5 bases upstream of the transcription start site of *CG31660* (Figure 1A). Details of the excision and molecular mapping are described in *Materials and Methods*. RT-PCR analysis of Δ181 showed that these mutants express a truncated transcript corresponding to residues 1–248 of the protein sequence. A full-length transcript was not detected in the mutants—a result consistent with the molecular nature of the mutation (Supporting Information, Figure S1, C and D). Using RT-PCR, we also confirmed that the deletion in Δ181 does not affect expression of the neighboring *pog* gene (Figure S1E).

Homozygous $Dmon1^{\Delta 181}$ mutants die throughout development and during eclosion. The escaper adults are weak and usually die within 7 days. We measured the life span of $Dmon1^{\Delta 181}$ mutants as homozygotes and in combination with the deficiencies that span the locus. Homozygous $Dmon1^{\Delta 181}$ mutants show a severe lifespan defect: 50% of the animals survive <5 days. In case of $Dmon1^{\Delta 181}/Df(2L)9062$ and $Dmon1^{\Delta 181}/Df(2L)6010$, the half-life of the animals was approximately 7 and 18 days, respectively (Figure 1B). Expression of a HA-tagged *Dmon1* (*UAS-Dmon1::HA*) using the pan-neuronal driver *C155*-GAL4, rescued the life span defect in $Dmon1^{\Delta 181}/Df(2L)9062$ mutants (Figure 1B), indicating that lethality and reduced life span were due to loss of *Dmon1*.

Dmon1 mutants that eclose are slow and unable to climb. We quantified this defect by measuring the climbing speed and climbing ability of $Dmon1^{\Delta 181}$ and $Dmon1^{\Delta 181}/Df(2L)9062$ mutant animals 24 hr posteclosion. Wild-type and $Dmon1^{\Delta 181}/+$ animals did not show any significant difference in their average climbing speed [2.18 ± 0.48 (n = 34) sec *vs.* 2.5 ± 0.66 (n = 48) sec, respectively]. No significant change in speed was observed on day 5 [2.32 ± 0.58 (n = 34) *vs.* 2.77 ± 0.88 (n = 46) cm/sec, respectively] and day 8 [2.18 ± 0.51 (n = 34) *vs.* 2.32 ± 0.58 (n = 25), respectively] either. In contrast, the climbing speed of homozygous $Dmon1^{\Delta 181}$, $Dmon1^{\Delta 181}/Df(2L)9062$, and *C155*-GAL4; $Dmon1^{\Delta 181}/Df(2L)9062$ animals was significantly lower on day 1 [0.37 ± 0.28 (n = 21), 0.47 ± 0.23 (n = 31), and 0.42 ± 0.27 (n = 36) cm/sec, respectively; $P < 0.001$]. Pan-neuronal expression of *Dmon1::HA* in $Dmon1^{\Delta 181}/Df(2L)9062$ rescued this defect: the average climbing speed of these animals (*C155*-GAL4; $Dmon1^{\Delta 181}/Df(2L)9062$; *UAS-Dmon1*::HA) was comparable to wild type [2.23 ± 0.64 cm/sec, (n = 44) (Figure 1C) even though a small decrease in speed was observed on day 5 (2.03 ± 0.64 cm/sec, (n = 42)] and day 8 [1.79 ± 0.38 cm/sec, (n = 39)]. We measured climbing ability of the mutants by calculating the percentage of flies able to climb 6 cm in 5 sec. In wild-type and $Dmon1^{\Delta 181}/+$ animals, >97% and 98% of the flies, respectively, were able to climb this distance in the specified time, whereas <10% of $Dmon1^{\Delta 181}$, $Dmon1^{\Delta 181}/Df(2L)9062$, and *C155*-GAL4;$Dmon1^{\Delta 181}/Df(2L)9062$ animals showed robust climbing ability (Figure 1D). Neuronal expression of Mon1::HA using *C155*-GAL4 restored climbing ability to wild-type levels (98%, Figure 1D). Thus, despite the difference in severity of lifespan between homozygous $Dmon1^{\Delta 181}$ and $Dmon1^{\Delta 181}$/deficiency animals, there seemed to be little difference in their motor abilities. $Dmon1^{\Delta 181}$ mutants express a truncated transcript that encodes the longin domain. The longin domain of Mon1 is known to form homodimers with itself and heterodimers with the longin domain of its partner protein, CCZ1. It is possible that formation of nonfunctional dimers in $Dmon1^{\Delta 181}$ contributes to the increased serverity in lifespan (Nordmann *et al.* 2010).

Dmon1 mutants show accumulation of Rab5 positive endosomes: In *Drosophila* and *C. elegans* loss of Mon1/SAND1 leads to accumulation of Rab5. These mutants also fail to recruit Rab7 onto endosomes (Poteryaev *et al.* 2007, 2010; Kinchen and Ravichandran 2010). To determine if homozygous $Dmon1^{\Delta 181}$ mutants exhibit a similar phenotype, we immunostained larval fillets for Rab5. In wild-type animals, small Rab5 positive puncta were seen distributed over the muscle (Figure 2, B and C, white arrows in B) and in the presynaptic regions (Figure 2, B and C, yellow arrows). In comparison, $Dmon1^{\Delta 181}$ mutants showed large scattered aggregates of Rab5, representing enlarged endosomes (Figure 2, E and F, arrows). Similar Rab5 positive puncta were also seen in $Dmon1^{\Delta 181}/Df(2L)9062$ and $Dmon1^{\Delta 181}/Df(2L)6010$ animals albeit smaller in size compared to $Dmon1^{\Delta 181}$ (data not shown). Similar to Rab5, expression of Rab7 in muscles appeared punctate in wild-type larvae, suggesting vesicular localization (Figure 2H, inset); however, in $Dmon1^{\Delta 181}$ mutants, Rab7 staining appeared more diffuse, suggesting that localization, but not expression, of this protein is likely to be affected (Figure 2K, inset). These results are consistent with the previous observations made in *Drosophila* and *C. elegans*, thus validating our loss-of-function allele (Kinchen and Ravichandran 2010; Yousefian *et al.* 2013).

$Dmon1^{\Delta 181}$ mutants exhibit altered synaptic morphology at the NMJ: The strong motor defect in $Dmon1^{\Delta 181}$ led us to examine the mutants for possible synaptic defects. A distinct change in synaptic morphology was observed at the neuromuscular junction in third instar larvae: most often, the

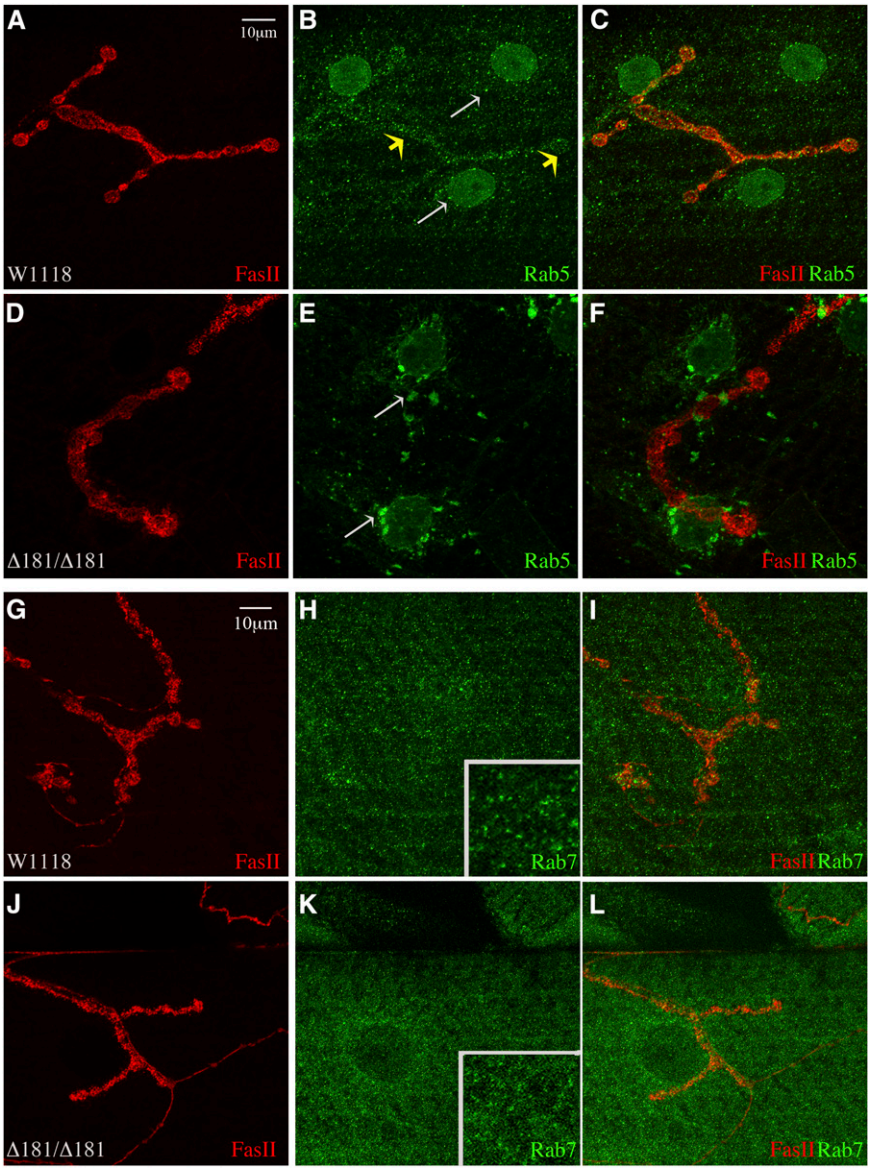

Figure 2 Altered Rab5 and Rab7 staining observed in *Dmon1*$^{\Delta 181}$ mutants. (A–C) Muscle 4 synapse of w1118 stained with FasII (red) and anti-Rab5 (green). Small Rab5 positive puncta are seen in the presynaptic terminal (yellow arrows) and in muscles (white arrows). (D–F) *Dmon1*$^{\Delta 181}$mutant. Rab5 positive aggregates are seen in the muscle and perinuclear regions (arrows in E). (G–L) NMJ at muscle 4 stained with FasII (red) and anti-Rab7 (green). (G–I) Small intense Rab7 punctae are present distributed over the muscle (H and inset) in w1118. In *Dmon1*$^{\Delta 181}$ animals (J–L), Rab7 staining appears more diffuse than punctate (K and inset).

boutons appeared large and surrounded by smaller supernumerary boutons (Figure 3, D–F, arrows in inset). At times, the boutons appeared odd shaped, indicating fusion of two adjacent boutons (Figure 3D, asterisk). Bouton size in mutant synapses was measured and compared to wild type by calculating the average diameter of boutons per synapse. In *Dmon1*$^{\Delta 181}$ mutants the average bouton size was significantly larger (3N; 5.46 ± 0.74 μm, $P < 0.001$) than wild type (3N; 4.016 ± 0.75 μm). Despite the difference in size, we did not observe any significant difference in bouton number between the two genotypes [10.87 ± 3.46 (wild type) and 12 ± 3.7 (*Dmon1*$^{\Delta 181}$)].

The number of satellite boutons was also scored in these mutants. *Dmon1*$^{\Delta 181}$ animals showed a 250% increase in satellite boutons (5.6 ± 2.57 in *Dmon1*$^{\Delta 181}$ *vs.* 1.61 ± 1.66 in wild type). A similar increase was observed in *Dmon1*$^{\Delta 181}$*/Df(2L)9062* (7.38 ± 3.01, 360%) and *Dmon1*$^{\Delta 181}$*/Df (2L)6010* animals (6.26 ± 2.51, 290%), confirming that the phenotype is indeed due to loss of *Dmon1* (Figure 3M).

Neuronal knockdown of *Dmon1* using RNAi also led to an increase in bouton size (Figure 3, J–L) with the average size being 4.78 ± 0.55 μm ($P < 0.001$) compared to 3.26 ± 0.49 μm in control animals (Figure 3N). However, unlike *Dmon1*$^{\Delta 181}$, satellite boutons were not observed in these animals, suggesting that neuronal knockdown of *Dmon1* alone may not be sufficient to give rise to the phenotype.

Expression of synaptic proteins Bruchpilot, GluRIIA, and GluRIIB is altered in Dmon1$^{\Delta 181}$ mutants: Mutations in trafficking genes are known to affect synaptic growth and neurotransmission (Littleton and Bellen 1995; Sanyal and Ramaswami 2002; Sweeney and Davis 2002; Dermaut *et al.* 2005). To further characterize the synaptic phenotype in *Dmon1* mutants, expression of presynaptic and postsynaptic markers was examined using immunostaining. Bruchpilot

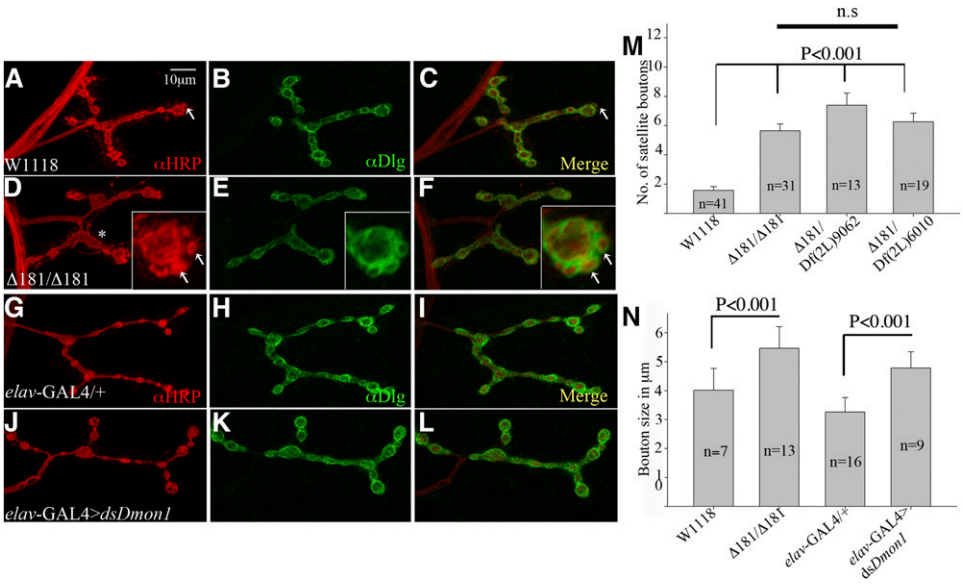

Figure 3 *Dmon1* mutants show altered synaptic morphology. A muscle 4 synapse. (A–C) w1118 and (D–F) *Dmon1*$^{\Delta 181}$ mutant immunostained with anti-HRP (red) and anti-Dlg (green). Arrow in A and C shows a satellite bouton sometimes seen in wild type. (B and C) Dlg staining seen as a tight ring around the presynapse. (D) *Dmon1*$^{\Delta 181}$ mutants show larger, sometimes odd-shaped boutons (asterisk). Small satellite boutons are seen surrounding larger boutons (insets in D–F, arrows). (E and F) Dlg staining is unaltered in the mutants (E and F). (G–I) *elav*-GAL4/+ and (J–L) *elav*-GAL4 > *UAS-dsDmon1* animals immunostained with anti-HRP (red) and anti-Dlg (green). Expression of ds*Dmon1* results in bigger boutons (J). (M) Quantitation of satellite bouton number. Average number per synapse observed in w1118 is 1.61 ± 1.66 (wild type, n = 41). *Dmon1*$^{\Delta 181}$, *Dmon1*$^{\Delta 181}$/*Df(2L)9062*, and *Dmon1*$^{\Delta 181}$/*Df(2L)6010* animals show 5.6 ± 2.57, 7.38 ± 3.01, and 6.26 ± 2.51 satellite boutons per synapse, respectively ($P < 0.001$). (N) Quantitation of bouton size in wild type and *Dmon1* mutants. The average bouton diameter (5.46 ± 0.74 μm) in *Dmon1*$^{\Delta 181}$ animals is significantly larger than in wild type (4.01 ± 0.75 μm). Expression of *dsDmon1* in neurons results in larger boutons (4.78 ± 0.55 μm) compared to controls (3.26 ± 0.49 μm). Error bars represent SD.

(Brp; mAb nc82) is a core protein involved in the assembly of active zones at the presynapse (Wagh *et al.* 2006). Wild-type synapses showed strong punctate expression of Brp (Figure 4, A–C, inset in C). In homozygous *Dmon1*$^{\Delta 181}$ mutants, a significant decrease in size (17.6%) and intensity (23%) of these puncta was observed (Figure 4, D–H).

Next, we checked if glutamate receptor levels at postsynaptic densities were altered in *Dmon1*$^{\Delta 181}$ mutants. Synapses at the larval neuromuscular junction are glutamatergic. The postsynaptic ionotropic glutamate receptor consists of four subunits. Of these, subunits GluRIIC, GluRIID, and GluRIIE are invariant, with the fourth subunit being either GluRIIA or GluRIIB. Thus, two classes of glutamate receptor clusters are present at the synapse: those containing GluRIIA and others with GluRIIB (Marrus and DiAntonio 2004; Marrus *et al.* 2004). Interestingly, the mutants showed a strong increase in the intensity of GluRIIA staining (Figure 4, L–N, inset in N). GluRIIA positive puncta were also seen in the muscle or extrasynaptic sites (Figure 4M). We measured the increase in fluorescence intensity by calculating the average gray value of GluRIIA normalized to HRP (Menon *et al.* 2004). In *Dmon1*$^{\Delta 181}$ and *Dmon1*$^{\Delta 181}$*/Df(2L)6010* mutants, the increase in intensity was ~74% and 56%, respectively, while *Dmon1*$^{\Delta 181}$*/Df(2L)9062* animals showed a 98% increase in GluRIIA intensity (Figure 4O).

The levels of GluRIIA and GluRIIB are reciprocally regulated at the synapse: an increase in GluRIIA leads to a decrease in GluRIIB (Petersen *et al.* 1997; DiAntonio *et al.* 1999; Sigrist *et al.* 2002; DiAntonio and Hicke 2004). We therefore checked *Dmon1* mutants for expression of GluRIIB to determine if the mutation affected both GluR subunits. Consistent with the reciprocal regulation of these receptor subunits, homozygous *Dmon1*$^{\Delta 181}$ mutants showed a distinct decrease in the intensity of GluRIIB at the synapse and absence of any extrasynaptic expression of the protein (Figure 4, S–U and U′). We measured the decrease in fluorescence intensity of GluRIIB normalized to FasciclinII, whose level seemed comparable between wild-type and mutant animals. *Dmon1*$^{\Delta 181}$ mutants showed a 42% decrease in the intensity of GluRIIB, indicating the increase in receptor levels to be specific to GluRIIA, and that the mechanism controlling the homeostasis between GluRIIA and GluRIIB is unaffected.

We checked whether the increase in GluRIIA is due transcriptional up-regulation of the gene, by carrying out quantitative reverse transcriptase PCR. Interestingly, we did not observe any significant difference in transcript levels between wild-type and *Dmon1*$^{\Delta 181}$ animals. The calculated average fold difference was 1 and 0.89 ± 0.22 (P = 0.47), respectively, suggesting that the specific increase in GluRIIA levels in the mutants is likely to be largely due to loss of posttranscriptional regulation.

Loss of neuronal Dmon1 is sufficient to alter the level of GluRIIA: Next, to determine the relative contribution of the pre- and postsynaptic compartments to the GluRIIA phenotype, RNAi was used to down-regulate *Dmon1* in neurons and muscles. Compared to wild type (Figure 5, A–C, arrow in inset), expression of *Dmon1* dsRNA using *C155*-GAL4; *elav*-GAL4 line—a line carrying two copies of the panneuronal GAL4—resulted in a 70% increase in fluorescence intensity of GluRIIA (Figure 5, E–G) while a 32% increase was seen upon knockdown using the motor neuron-specific *OK6*-GAL4 (Figure 5N). In both experiments, an increase in GluRIIA positive extrasynaptic punctae was also observed. These

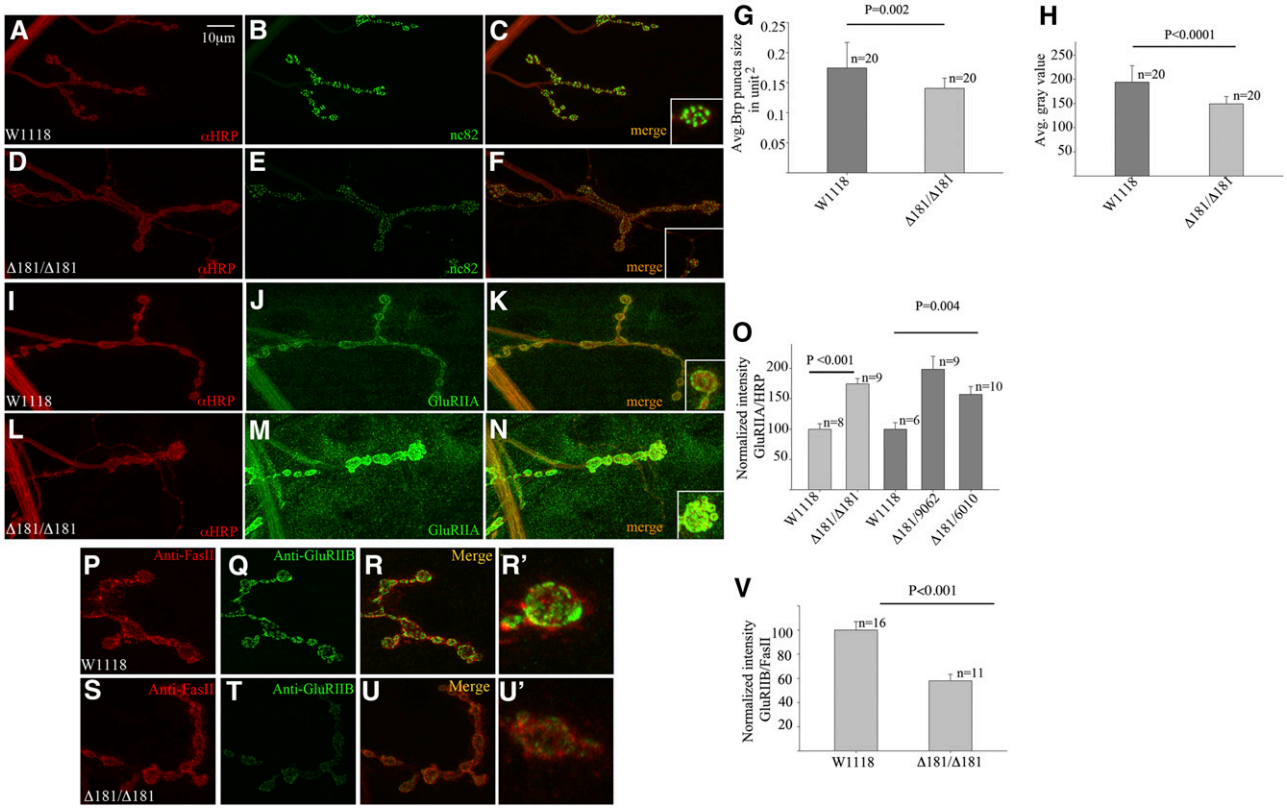

Figure 4 Expression levels of Brp and GluRIIA are altered in *Dmon1*$^{\Delta 181}$ mutants. (A–F) Synapse at muscle 4 stained with anti-HRP (red) and mAb nc82 (anti-Brp, green) in w1118 animal (A–C) and homozygous *Dmon1*$^{\Delta 181}$ mutant (D–F). Intensity of Brp staining is low (inset in F). (G) Size of nc82 postive puncta in *Dmon1*$^{\Delta 181}$ mutants is 17.6% smaller than wild type ($P = 0.002$). (H) Intensity of nc82 puncta in *Dmon1*$^{\Delta 181}$ mutants is 23% less compared to wild type. (I–N) NMJ at muscle 4 stained with anti-HRP (red) and GluRIIA (green). (I–K) w1118 synapse. (L–N) Homozygous *Dmon1*$^{\Delta 181}$. Elevated GluRIIA expression is seen at the synapse and muscles. (O) Quantification of GluRIIA intensity normalized to HRP. Homozygous *Dmon1*$^{\Delta 181}$ mutants show a 74% increase in intensity compared to wild type. *Dmon1*$^{\Delta 181}$*/Df(2L)6010* and *Dmon1*$^{\Delta 181}$*/Df(2L)9062* animals show a 56% and 98% increase, respectively. Error bars represent SEM. (P–U) NMJ at muscle 4 immunostained with anti-FasII (red) and anti-GluRIIB (green). (P–R and R′) w1118 synapse. (S–U and U′) *Dmon1*$^{\Delta 181}$ mutant. GluRIIB expression is reduced. (V) Quantification of GluRIIB intensity normalized to anti-FasII. *Dmon1*$^{\Delta 181}$ mutants show a 42% decrease in GluRIIB compared to wild type. Error bars represent SEM.

results thus suggest that loss of *Dmon1* in the presynaptic compartment is sufficient to trigger postsynaptic increase in GluRIIA.

To determine if neuronal overexpression of *Dmon1* has an opposite effect on GluRIIA levels, we overexpressed *UAS-Dmon1*::*HA* using the *C155*-GAL4; *elav*-GAL4 line. A 24% decrease in receptor levels was observed (Figure 5, G, L, and M). A decrease in receptor levels was also observed when the *Dmon1* was overexpressed in the muscle (data not shown). This indicates that while loss of neuronal *Dmon1* is sufficient to phenocopy the mutant GluRIIA phenotype, receptor levels can be modulated pre and postsynaptically by DMon1.

The synaptic phenotypes in Dmon1 mutants can be rescued by pre- and postsynaptic expression of Dmon1: To further confirm that the increase in GluRIIA is indeed due to loss of *Dmon1*, we checked if expression of the gene in the mutants rescues the synaptic phenotype. We expressed *UAS-Dmon1*::*HA* presynaptically in homozygous *Dmon1*$^{\Delta 181}$ and *Dmon1*$^{\Delta 181}$*/Df(2L)9062* larvae and examined the receptor levels in these animals. Compared to mutants (*Dmon1*$^{\Delta 181}$, *elav*-GAL4*/Dmon1*$^{\Delta 181}$; Figure 6, A–C and C′), "rescue" animals expressing *UAS-Dmon1*::*HA*, showed a 48% decrease in the intensity of GluRIIA (Figure 6, D–G). A significant decrease (27%) in GluRIIA levels was also observed in *Dmon1*$^{\Delta 181}$*/Df(2L)9062* mutants expressing *Dmon1*::*HA* (Figure 6N). Given the role of DMon1 in regulating endosomal trafficking it seemed possible that impaired cellular trafficking in the muscle might contribute to the increased accumulation of GluRIIA at the synapse. We therefore checked if postsynaptic expression of *Dmon1* could rescue the GluRIIA phenotype. Expression of GluRIIA was significantly lowered in the "muscle-rescue" animals (Figure 6, K–M and M′). A near 70% decrease in the synaptic levels of GluRIIA was observed in these animals (0.12 ± 0.05 in rescue *vs.* 0.39 ± 0.15 in mutant control) (Figure 6N).

Interestingly, both presynaptic and postsynaptic expression of *Dmon1* rescued the satellite bouton phenotype seen in the mutants (Figure 6O). Neuronal rescue of *Dmon1*$^{\Delta 181}$*/Df(2L)9062* led to a 75% decrease in the number of satellite boutons (3.76 ± 1.99 in mutant *vs.* 0.95 ± 1.24 in neuronal rescue). A

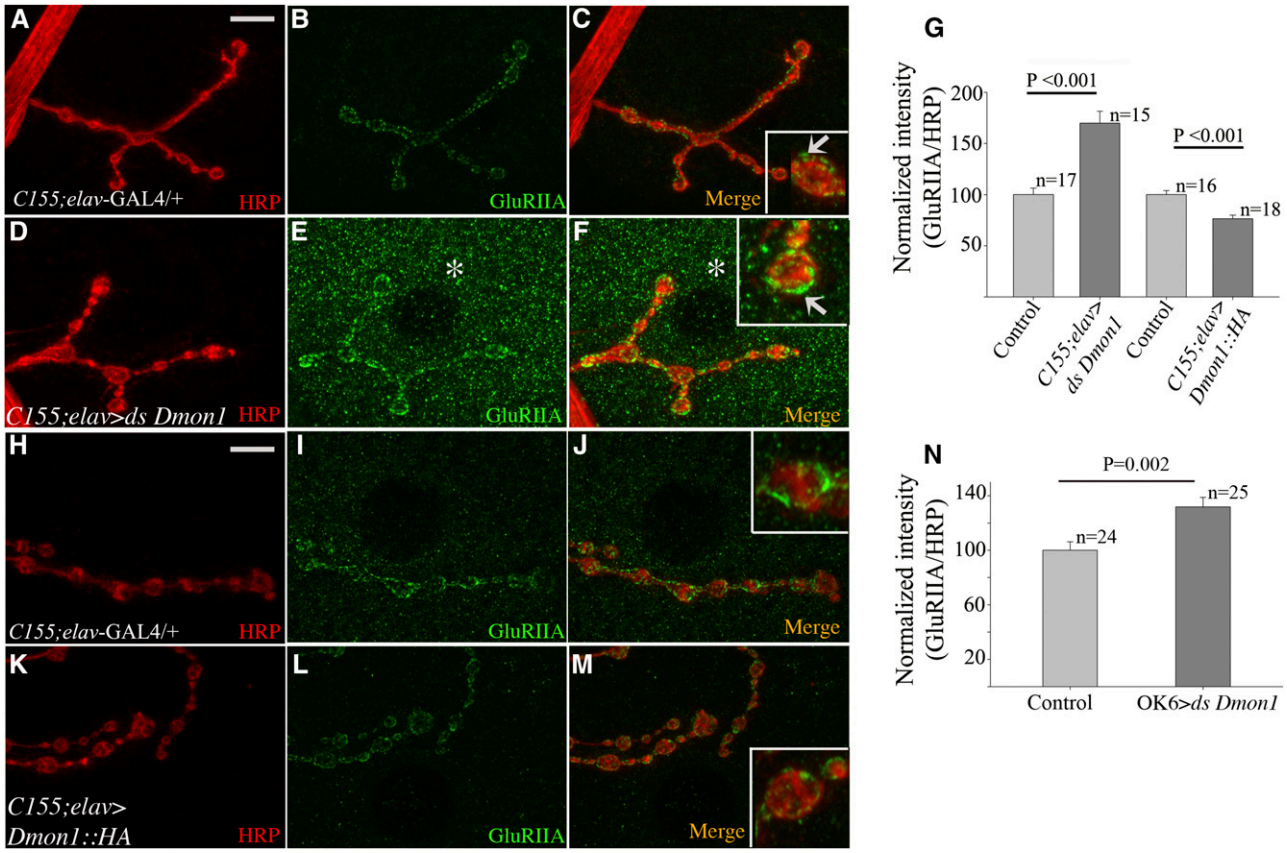

Figure 5 Loss of neuronal *Dmon1* increases GluRIIA levels at synaptic and extrasynaptic sites. (A–C and H–J) Control (*C155*-Gal4/+; *elav*-GAL4/+) synapse at muscle 4 immunostained with anti-HRP (red) and anti-GluRIIA (green). (D–F) Presynaptic knockdown of *Dmon1* increases intensity of GluRIIA staining at the NMJ (F, arrow in inset). Increase in extrasynaptic GluRIIA punctae is observed (E and F, asterisk). (G) Normalized GluRIIA:HRP intensity for *Dmon1* RNAi and UAS-Dmon1::HA animals. RNAi animals show a 70% increase in intensity. (K–M) Neuronal overexpression of Dmon1:HA leads to decrease in intensity of GluRIIA (L, inset in M) by 24% (G). (N) A 32% increase in GluRIIA expression was observed in *OK6-GAL4 > UAS-Dmon1RNAi* animals. Error bars represent SEM.

comparable decrease (80%) was observed in mutants expressing *Dmon1* postsynaptically (4.25 ± 2.51 in mutant "control" *vs.* 0.80 ± 1.6 in muscle rescue larvae) (Figure 6O). Together, these results indicate that the synaptic phenotypes in *Dmon1* mutants is indeed due to loss of the gene, and both presynaptic as well as postsynaptic expression of the gene can rescue these defects.

DMon1 is secreted at the neuromuscular junction: A study of the localization of Rabs in the ventral ganglion of third instar larvae suggests differential localization of each of these proteins (Chan *et al.* 2011). Components of the endocytic machinery are also present at the NMJ and regulate vesicle recycling and formation of active zone complexes (Wucherpfennig *et al.* 2003; Graf *et al.*, 2009). To determine if DMon1 might play a role in any of the above processes, we sought to determine if the protein localizes to the synapse. We expressed *UAS-Dmon1::HA* in neurons and stained larval fillets using antibodies against the HA tag. In control (*UAS-Dmon1::HA/+*) animals, a few small puncta were seen dispersed around the area of the boutons (Figure 7, A–C and C′). Interestingly, in *elav*-GAL4>*UAS-Dmon1::HA* animals, strong HA positive puncta were observed surrounding the bouton (Figure 7, D–F and F′). The perisynaptic localization of Dmon1 was also observed when *OK6*-GAL4 was used to drive expression of *UAS-Dmon1::HA*. To visualize the localization of DMon::HA more clearly, a 3D rendering of the images were examined. As shown in Figure 7F′′ and F′′′, HA positive puncta were seen to be clearly surrounding the HRP positive presynaptic compartment. To further rule out possible staining artifacts caused by overexpression, localization of DMon1::HA was examined in $Dmon1^{\Delta 181}/Df(2L)9062$ animals. Expression of DMon1::HA in a *Dmon1* mutant background was also found to be perisynaptic, suggesting that the localization is unlikely to be an artifact caused by overexpression, although this needs to be tested more rigorously (Figure S3). We tried to determine if the localization of DMon1 is dependent on Rab11 since it is required for exosomal secretion (Raposo and Stoorvogel 2013). To do this, we coexpressed the tagged transgene with dominant negative Rab11 (DN-Rab11) in neurons. However, coexpression with DN-Rab11 led to widespread lethality, making it difficult evaluate this interaction.

We also examined anti-Dlg staining in animals overexpressing *Dmon1*. As opposed to the usual tight ring seen in

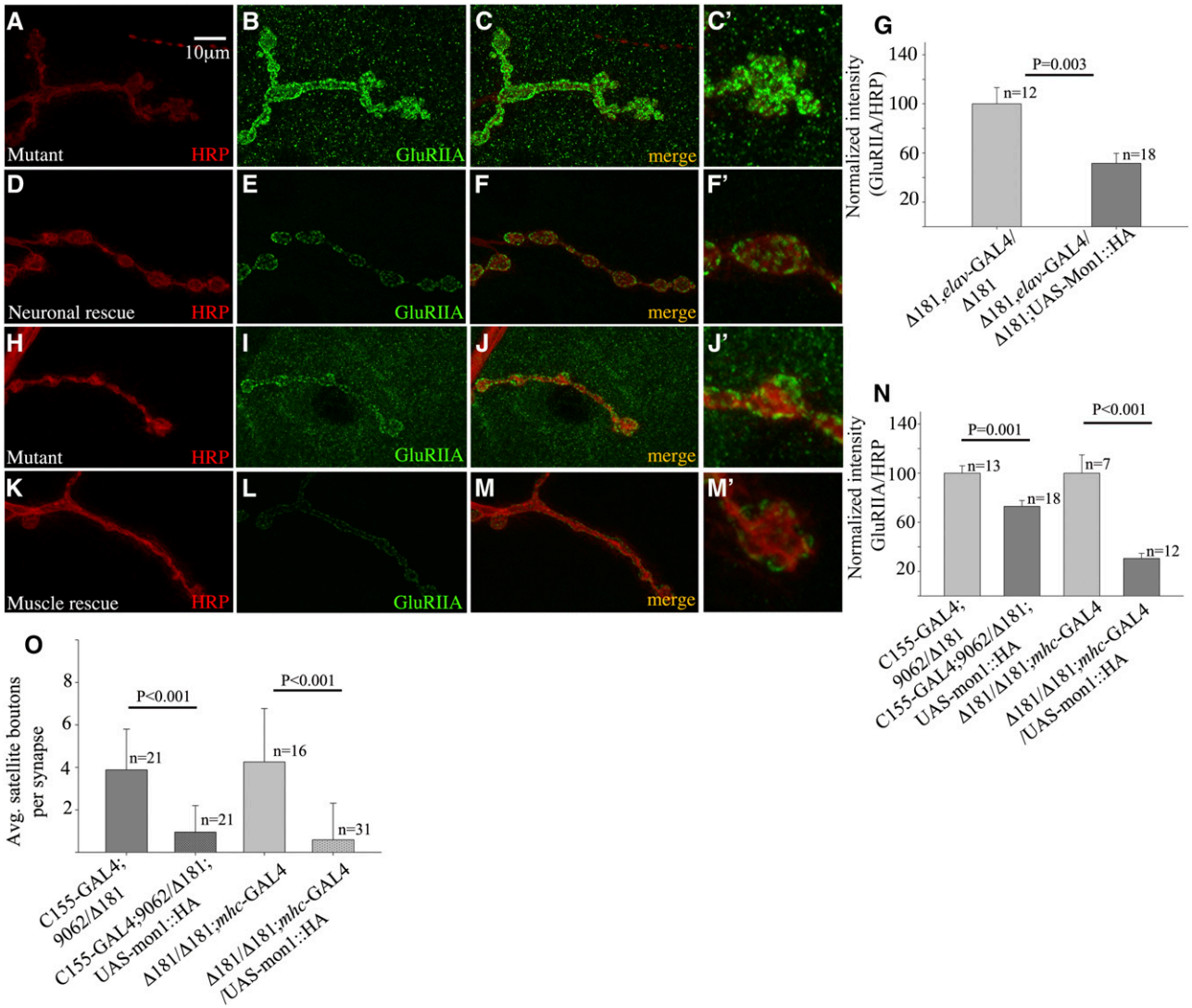

Figure 6 Presynaptic and postsynaptic expression of *Dmon1* rescues the GluRIIA phenotype in *Dmon1* mutants. (A–C and C′) Control animal (*Dmon1*$^{\Delta 181}$, *elav*-GAL4/*Dmon1*$^{\Delta 181}$) with intense GluRIIA staining at the NMJ and muscles (C′). (D–F) Neuronal expression of *Dmon1*::*HA* in *Dmon1*$^{\Delta 181}$ mutants rescues the GluRIIA phenotype (F and F′). (G) Normalized GluRIIA:HRP intensity. The intensity of GluRIIA is reduced by 48% in rescue animals. Error bars represent SEM. (N) Neuronal expression of *UAS-Dmon1:HA* in *Dmon1*$^{\Delta 181}$/*Df(2L)9062* leads to a 27% decrease in GluRIIA levels. Error bars represent SEM. (H–J and J′) Control (*Dmon1*$^{\Delta 181}$/*Dmon1*$^{\Delta 181}$; *mhc*-GAL4/+) synapse. HRP (red) and GluRIIA (green). (K–M and M′) Postsynaptic expression of *Dmon1*::*HA* in *Dmon1*$^{\Delta 181}$ animals down-regulates GluRIIA expression. (N) Normalized GluRIIA:HRP intensity. A 70% decrease in intensity is observed in muscle-rescue animals. (O) Quantification of the satellite boutons. Fewer satellite boutons are observed in rescue animals. Error bars represent standard deviation (SD).

control animals (Figure 7, G–I and I′), Dlg staining was found to be broad and diffuse in animals overexpressing *Dmon1*::*HA* (Figure 7, J–L and L′). These results suggest that DMon1 localizes to the synapse and is likely to be released from the presynaptic compartment.

Neurotransmitter vesicle size is reduced in Dmon1 mutants: Expression of GluRIIA is dependent on cell–cell contact between the nerve and muscle (Karr *et al.* 2009; Ganesan *et al.* 2011; Fukui *et al.* 2012). Further, homeostatic mechanisms regulate neurotransmitter release and postsynaptic receptor composition and density in response to presynaptic activity (Petersen *et al.* 1997; Davis *et al.* 1998; Schmid *et al.* 2008). To gain further insight into the possible cause of increased GluRIIA accumulation, we examined the ultrastructure of boutons from wild type and *Dmon1*$^{\Delta 181}$ mutants. Interestingly, the mutants showed a distinct decrease in the size of synaptic vesicles (Figure 8, B and C). In wild type, the average vesicle diameter measured 40.35 ± 5.32 nm—a value comparable to what has been previously observed (Daniels *et al.* 2006); the mutants showed a 28.77% decrease in diameter with the average diameter being 28.74 ± 7 nm.

One of the factors regulating vesicle size is *dvglut*, which encodes the vesicular glutamate transporter. Loss of *dvglut* leads to a decrease in size of synaptic vesicles while overexpression results in an increase in vesicle size and amplitude

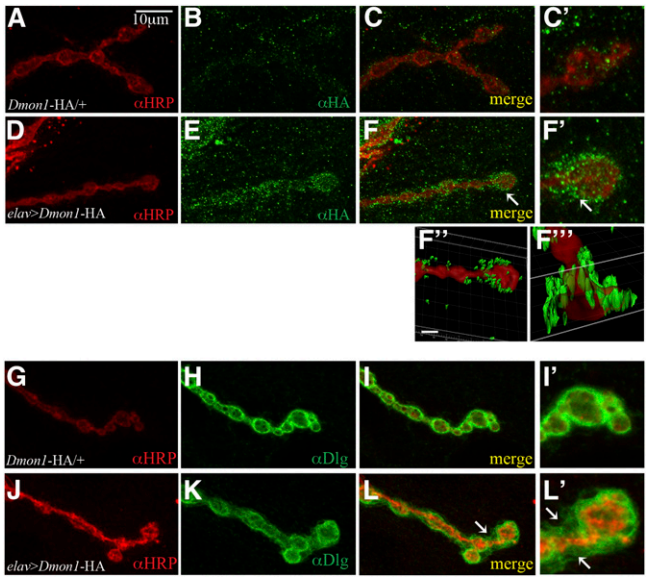

Figure 7 DMon1 localization is perisynaptic. (A–C and C′). Control animal (*UAS-Dmon1::HA/+*) stained with anti-HRP (red) and anti-HA antibody (green). A few green puncta are seen in the background (C and C′). (D–F) *elav*-GAL4 > *UAS-Dmon1::HA* animal. HA positive puncta are seen surrounding the bouton (F and F′). A 3D volume rendering of the image and its cross-section shows HA positive puncta to be surrounding the bouton (F′′ and F′′′). (G–I) Anti-HRP (red) and anti-Dlg (green) staining in control (*UAS-Dmon1::HA/+*) and *elav*-GAL4 > *UAS-Dmon1::HA* (J–L) animals. Note the diffuse Dlg staining in *elav*-GAL4 > *UAS-Dmon1::HA* (K, L, and L′).

of spontaneous release (Daniels *et al.* 2004, 2006). We did not observe any significant change in vGlut/FasII ratios in $Dmon1^{\Delta 181}$ (2.05 ± 0.67 in W1118 *vs.* 1.85 ± 0.72 in $Dmon1^{\Delta 181}$). To determine if increasing glutamate release can down-regulate GluRIIA expression, we overexpressed *dvglut* in *Dmon1* mutants and examined its effect on GluRIIA levels. Indeed, presynaptic overexpression of vglut in $Dmon1^{\Delta 181}/Df(2L)9062$ animals resulted in a 49% decrease in postsynaptic GluRIIA levels and loss of extrasynaptic GluRIIA (Figure 8, G–I and J). A comparable decrease (43%) in receptor levels was observed when overexpression was carried out in a $Dmon1^{\Delta 181}$ background (Figure 8J). Expression of vGlut also suppressed the satellite bouton phenotype in *Dmon1* mutants (Figure 8K). A 50% decrease in satellite bouton number was observed in $Dmon1^{\Delta 181}/Df(2L)9062$ animals [control (4.82 ± 2.6) *vs.* rescue (2.24 ± 1.71)] while a 80% decrease was observed in homozygous $Dmon1^{\Delta 181}$ animals [mutant control (7.23 ± 3.21) *vs.* rescue (1.33 ± 1.34)]. This suggests that altered glutamate release in *Dmon1* mutants could contribute to the increase in GluRIIA levels and postsynaptic homeostatic mechanisms are not affected in these mutants.

Discussion

Neurotransmitter release at the synapse is modulated by factors that control synaptic growth, synaptic vesicle recycling, and receptor turnover at postsynaptic sites (Sweeney and Davis 2002; Glodowski *et al.* 2007; Kim and Kandler 2010; Fernandes *et al.* 2014). Endolysosomal trafficking modulates the function of these factors and therefore plays an important role in regulating synaptic development and function. Intracellular trafficking is regulated by Rabs, which are small GTPases. These proteins control specific steps in the trafficking process. A clear understanding of the role of Rabs at the synapse is still nascent. *Drosophila* has 31 Rabs, and most of these are expressed in the nervous system (Chan *et al.* 2011). Rab5 and Rab7, present on early and late endosomes, respectively, are critical regulators of endolysosomal trafficking and loss of this regulation affects neuronal viability underscored by the fact that mutations in Rab7 are associated with neurodegeneration (Verhoeven *et al.* 2003). Rab5 along with Rab3 is present on synaptic vesicles, and both play a role in regulating neurotransmitter release (Fischer Von Mollard *et al.* 1994a,b; Sudhof 1995). In *Drosophila*, Rab3 is involved in the assembly of active zones by controlling the level of both Bruchpilot—a core active zone protein—and the calcium channels surrounding the active zone (Graf *et al.* 2009). In hippocampal and cortex neurons, Rab5 facilitates LTD through removal of AMPA receptors from the synapse (Brown *et al.* 2005; Zhong *et al.* 2008). In *Drosophila*, Rab5 regulates neurotransmission; it also functions to maintain synaptic vesicle size by preventing homotypic fusion (Shimizu *et al.* 2003; Wucherpfennig *et al.* 2003). Compared to Rab5 or Rab3, less is known about the roles of Rab7 at the synapse. In spinal cord motor neurons, Rab7 mediates sorting and retrograde transport of neurotrophin-carrying vesicles (Deinhardt *et al.* 2006). In *Drosophila*, tbc1D17—a known GAP for Rab7—affects GluRIIA levels (Lee *et al.* 2013); the effect of this on neurotransmission has not been evaluated. Excessive trafficking via the endolysosomal pathway also affects neurotransmission. This has been observed in mutants for tbc1D24—a GAP for Rab35. A high rate of turnover of synaptic vesicle proteins in these mutants is seen to increase neurotransmitter release (Uytterhoeven *et al.* 2011; Fernandes *et al.* 2014).

In this study we have examined the synaptic role of DMon1—a key regulator of endosomal maturation. Multiple synaptic phenotypes are found associated with *Dmon1* loss of function, and one of these is altered synaptic morphology. Boutons in *Dmon1* mutants are larger with more satellite or supernumerary boutons (Figure 3)—a phenotype strongly associated with endocytic mutants (Dickman *et al.* 2006). Formation of satellite boutons is thought to occur due to loss of bouton maturation, with the initial step of bouton budding being controlled postsynaptically and the maturation step being regulated presynaptically (Lee and Wu 2010). Supporting this, a recent study shows that miniature neurotransmission is required for bouton maturation (Choi *et al.* 2014). The presence of excess satellite boutons in *Dmon1* mutants suggests that the number of "miniature" events is likely to be affected in these mutants. The fact that we can rescue this phenotype upon expression of vGlut supports this possibility

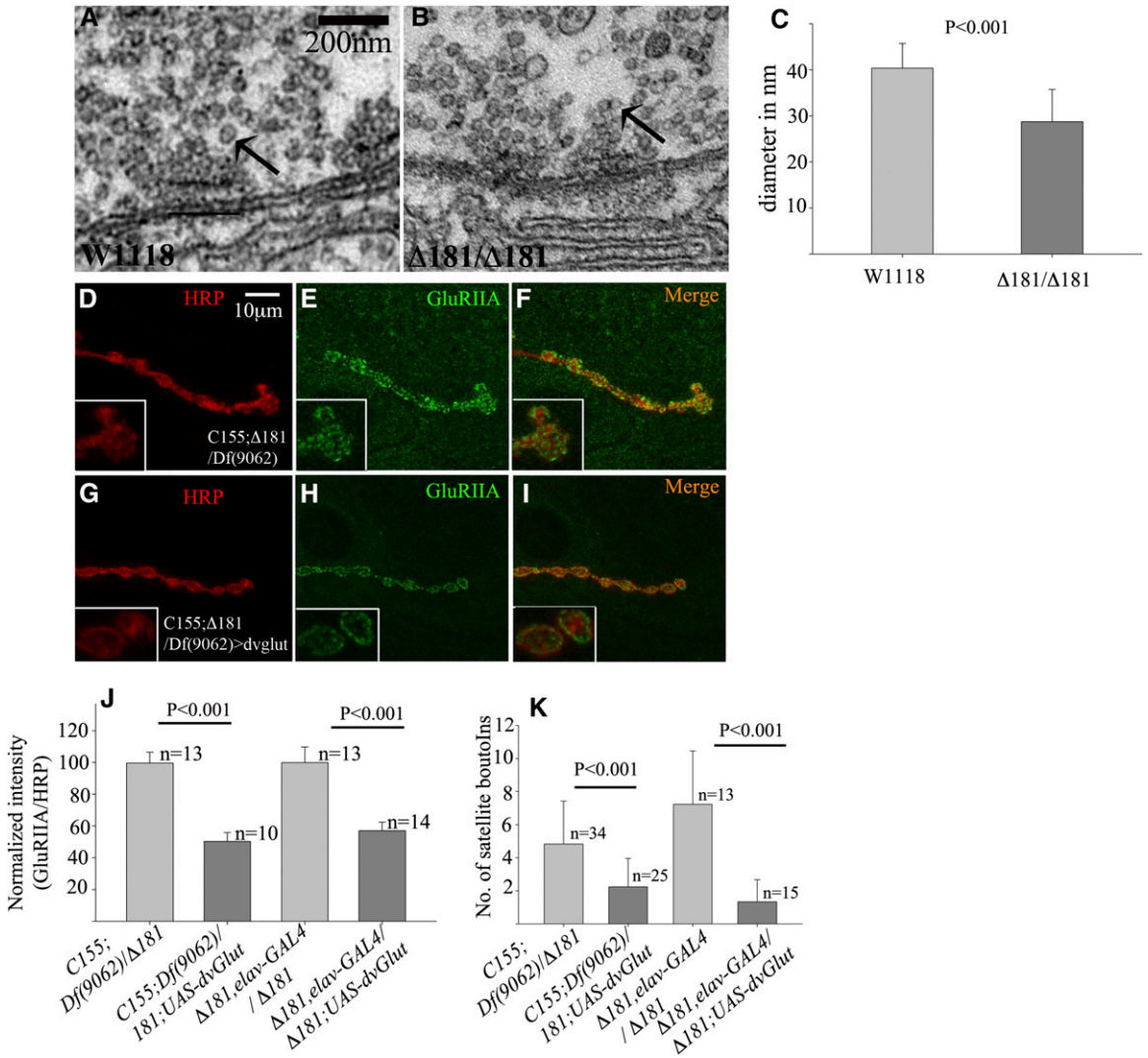

Figure 8 Expression of *dvglut* in *Dmon1* mutants suppresses the GluRIIA phenotype. (A and B) Electron micrograph of the active zone region of w1118 (A) and *Dmon1*$^{\Delta 181}$ mutant (B) at identical magnification. Synaptic vesicles (arrows in A and B) are smaller in the mutants. (C) Average vesicle diameter in mutants (28.74 ± 7 nm) is 28.7% smaller than wild type (40.35 ± 5.32 nm). (D–I) Control (C155; *Dmon1*$^{\Delta 181}$*/Df(2L)9062*) and mutants overexpressing *dvglut* stained with HRP (red) and anti-GluRIIA (green). (G–I) Expression of *UAS-dvGlut* decreases GluRIIA levels in the mutant (I and inset). Bar in A, 10 μm. (J) Normalized GluRIIA:HRP intensity. Overexpression of *dvglut* leads to a 49% and 43% decrease in GluRIIA levels in C155-GAL4;*Dmon1*$^{\Delta 181}$/Df (2L)9062 and *Dmon1*$^{\Delta 181}$, *elav*-GAL4/*Dmon1*$^{\Delta 181}$ animals, respectively. Error bars represent SEM. (K) Quantification of satellite bouton number in *Dmon1* mutants and mutants overexpressing *vglut*. A significant decrease in satellite boutons is observed in the mutants.

(Figure 8). However, this does not fit with the observed decrease in size and intensity of Brp positive puncta in these mutants. Active zones with low or nonfunctional Brp are known to be more strongly associated with increased spontaneous neurotransmission (Melom *et al.* 2013; Peled *et al.* 2014). Considering the involvement of postsynaptic signaling in initiating satellite bouton formation, we think altered neurotransmission possibly together with impaired postsynaptic or retrograde signaling, contributes to the altered synaptic morphology in *Dmon1* mutants. This may also explain why we fail to observe satellite boutons in neuronal RNAi animals.

A striking phenotype associated with loss of *Dmon1* is the increase in GluRIIA levels (Figure 4). This phenotype seems presynaptic in origin since neuronal loss of *Dmon1* is sufficient to increase GluRIIA levels (Figure 5). Is the increase in GluRIIA due to trafficking defects in the neuron? This seems unlikely for the following reasons: First, it has been shown that although neuronal overexpression of wild-type and dominant negative *Rab5* alters evoked response in a reciprocal manner, there is no change in synaptic morphology, glutamate receptor localization and density, or change in synaptic vesicle size (Wucherpfennig *et al.* 2003). The role of Rab7 at the synapse is less clear. In a recent study, loss of *tbc1D15-17*, which functions as a GAP for Rab7, was shown to increase GluRIIA levels at the synapse. Selective knockdown of the gene in muscles, and not neurons, was seen to increase GluRIIA levels, indicating that the function of the gene is primarily

postsynaptic (Lee *et al.* 2013). These data are not consistent with our results from neuronal knockdown of *Dmon1*, suggesting that the presynaptic role of *Dmon1* in regulating GluRIIA levels is likely to be independent of Rab5 and Rab7 and therefore novel.

Our experiments to evaluate the postsynaptic role of *Dmon1* have been less clear. Although we see a modest increase in GluRIIA levels upon knockdown in muscles, the increase is not always significant when compared to controls (data not shown). However, the fact that muscle expression of *Dmon1* can rescue the GluRIIA phenotype in the mutant (Figure 6) suggests that it is likely to be one of the players in regulating GluRIIA postsynaptically. Further, it is to be noted, that while overexpression of vGlut leads to down-regulation of the receptor at the synapse (Figure 8), the receptors do not seem to get trapped in the muscle, suggesting that multiple pathways are likely to be involved in regulating receptor turnover in the muscle, and the DMon1–Rab7-mediated pathway may be just one of them.

How might neuronal *Dmon1* regulate receptor expression? One possibility is that the increase in receptor levels is a postsynaptic homeostatic response to defects in neurotransmission, given that $Dmon1^{\Delta 181}$ mutants have smaller synaptic vesicles. However, in *dvglut* mutants, presence of smaller synaptic vesicles does not lead to any change in GluRIIA levels, given that receptors at the synapse are generally expressed at saturating levels (Daniels *et al.* 2006). Therefore, it seems unlikely that the increase in GluRIIA is part of a homeostatic response, although one cannot rule this out completely. The other possibility is that DMon1 is part of a transsynaptic signaling mechanism that regulates GluRIIA levels in a post-transcriptional manner. The observation that presynaptically expressed DMon1 localizes to postsynaptic regions (Figure 7) and our results from neuronal RNAi and rescue experiments support this possibility. The involvement of transsynaptic signaling in regulating synaptic growth and function has been demonstrated in the case of signaling molecules such as Ephrins, Wingless, and Syt4 (Contractor *et al.* 2002; Korkut and Budnik 2009; Korkut *et al.* 2013). In *Drosophila*, both Wingless and Syt4 are released by the presynaptic terminal via exosomes to mediate their effects in the postsynaptic compartment. We hypothesize that DMon1 released from the boutons either directly regulates GluRIIA levels or facilitates the release of an unknown factor required to maintain receptor levels. The function of DMon1 in the muscle is likely to be more consistent with its role in cellular trafficking and may mediate one of the pathways regulating GluRIIA turnover. These possibilities will need to be tested to gain a mechanistic understanding of receptor regulation by *Dmon1*.

Acknowledgments

We thank Thomas Klein, Jahan Forough Yousefian, Hermann Aberle and Aaron DiAntonio for antibodies and fly reagents; Gaiti Hasan, L. S. Shashidhara, and Richa Rikhy for helpful discussions; Girish Deshpande for critical comments; the Bloomington *Drosophila* Stock Center and the Vienna *Drosophila* RNAi Centre for fly stocks; the Bloomington *Drosophila* Genome Research Center for cDNA clones; the Indian Institute of Science Education and Research (IISER) for use of the microscopy facility; and National Centre for Biological Sciences (NCBS), Bangalore, and Centre for Cellular and Molecular Platforms (C-CAMP), Bangalore, for help with the TEM facility. This work was supported by funds from the Department of Biotechnology (DBT), Government of India (GOI), Agharkar Research Institute (ARI), Pune, to A.R.; Wellcome Trust DBT Indian Alliance (WT-DBT-IA) to G.S.R.; intramural funds from IISER to G.S.R.; Council of Industrial and Scientific Research, GOI, a Senior Research Fellowship to S.D.; and a fellowship from the University Grants Commission, GOI to Kumari Shweta. G.S.R. is a WT-DBT-IA Intermediate Fellow. Author contributions: A.R. conceived and designed the experiments; A.R., S.D., A.B., K.S., and P.S. performed the experiments; A.R., G.S.R., S.D., A.B., K.S. and P.S. analyzed the data; and A.R. and G.S.R. wrote the manuscript.

Literature Cited

Brown, T. C., I. C. Tran, D. S. Backos, and J. A. Esteban, 2005 NMDA receptor-dependent activation of the small GTPase Rab5 drives the removal of synaptic AMPA receptors during hippocampal LTD. Neuron 45: 81–94.

Chan, C. C., S. Scoggin, D. Wang, S. Cherry, T. Dembo *et al.*, 2011 Systematic discovery of Rab GTPases with synaptic functions in Drosophila. Curr. Biol. 21: 1704–1715.

Chinchore, Y., A. Mitra, and P. J. Dolph, 2009 Accumulation of rhodopsin in late endosomes triggers photoreceptor cell degeneration. PLoS Genet. 5: e1000377.

Choi, B. J., W. L. Imlach, W. Jiao, V. Wolfram, Y. Wu *et al.*, 2014 Miniature neurotransmission regulates Drosophila synaptic structural maturation. Neuron 82: 618–634.

Contractor, A., C. Rogers, C. Maron, M. Henkemeyer, G. T. Swanson *et al.*, 2002 Trans-synaptic Eph receptor-ephrin signaling in hippocampal mossy fiber LTP. Science 296: 1864–1869.

Daniels, R. W., C. A. Collins, M. V. Gelfand, J. Dant, E. S. Brooks *et al.*, 2004 Increased expression of the Drosophila vesicular glutamate transporter leads to excess glutamate release and a compensatory decrease in quantal content. J. Neurosci. 24: 10466–10474.

Daniels, R. W., C. A. Collins, K. Chen, M. V. Gelfand, D. E. Featherstone *et al.*, 2006 A single vesicular glutamate transporter is sufficient to fill a synaptic vesicle. Neuron 49: 11–16.

Davis, G. W., A. DiAntonio, S. A. Petersen, and C. S. Goodman, 1998 Postsynaptic PKA controls quantal size and reveals a retrograde signal that regulates presynaptic transmitter release in Drosophila. Neuron 20: 305–315.

Deinhardt, K., S. Salinas, C. Verastegui, R. Watson, D. Worth *et al.*, 2006 Rab5 and Rab7 control endocytic sorting along the axonal retrograde transport pathway. Neuron 52: 293–305.

Dermaut, B., K. K. Norga, A. Kania, P. Verstreken, H. Pan *et al.*, 2005 Aberrant lysosomal carbohydrate storage accompanies endocytic defects and neurodegeneration in Drosophila benchwarmer. J. Cell Biol. 170: 127–139.

DiAntonio, A., and L. Hicke, 2004 Ubiquitin-dependent regulation of the synapse. Annu. Rev. Neurosci. 27: 223–246.

DiAntonio, A., S. A. Petersen, M. Heckmann, and C. S. Goodman, 1999 Glutamate receptor expression regulates quantal size and quantal content at the Drosophila neuromuscular junction. J. Neurosci. 19: 3023–3032.

DiAntonio, A., A. P. Haghighi, S. L. Portman, J. D. Lee, A. M. Amaranto *et al.*, 2001 Ubiquitination-dependent mechanisms regulate synaptic growth and function. Nature 412: 449–452.

Dickman, D. K., Z. Lu, I. A. Meinertzhagen, and T. L. Schwarz, 2006 Altered synaptic development and active zone spacing in endocytosis mutants. Curr. Biol. 16: 591–598.

Dobie, F., and A. M. Craig, 2007 A fight for neurotransmission: SCRAPPER trashes RIM. Cell 130: 775–777.

Fernandes, A. C., V. Uytterhoeven, S. Kuenen, Y. C. Wang, J. R. Slabbaert *et al.*, 2014 Reduced synaptic vesicle protein degradation at lysosomes curbs TBC1D24/sky-induced neurodegeneration. J. Cell Biol. 207: 453–462.

Fernandez-Monreal, M., T. C. Brown, M. Royo, and J. A. Esteban, 2012 The balance between receptor recycling and trafficking toward lysosomes determines synaptic strength during long-term depression. J. Neurosci. 32: 13200–13205.

Fischer von Mollard, G., B. Stahl, C. Li, T. C. Sudhof, and R. Jahn, 1994a Rab proteins in regulated exocytosis. Trends Biochem. Sci. 19: 164–168.

Fischer von Mollard, G., B. Stahl, C. Walch-Solimena, K. Takei, L. Daniels *et al.*, 1994b Localization of Rab5 to synaptic vesicles identifies endosomal intermediate in synaptic vesicle recycling pathway. Eur. J. Cell Biol. 65: 319–326.

Fukui, A., M. Inaki, G. Tonoe, H. Hamatani, M. Homma *et al.*, 2012 Lola regulates glutamate receptor expression at the Drosophila neuromuscular junction. Biol. Open 1: 362–375.

Ganesan, S., J. E. Karr, and D. E. Featherstone, 2011 Drosophila glutamate receptor mRNA expression and mRNP particles. RNA Biol. 8: 771–781.

Glodowski, D. R., C. C. Chen, H. Schaefer, B. D. Grant, and C. Rongo, 2007 RAB-10 regulates glutamate receptor recycling in a cholesterol-dependent endocytosis pathway. Mol. Biol. Cell 18: 4387–4396.

Graf, E. R., R. W. Daniels, R. W. Burgess, T. L. Schwarz, and A. DiAntonio, 2009 Rab3 dynamically controls protein composition at active zones. Neuron 64: 663–677.

Heckscher, E. S., R. D. Fetter, K. W. Marek, S. D. Albin, and G. W. Davis, 2007 NF-kappaB, IkappaB, and IRAK control glutamate receptor density at the Drosophila NMJ. Neuron 55: 859–873.

Karr, J., V. Vagin, K. Chen, S. Ganesan, O. Olenkina *et al.*, 2009 Regulation of glutamate receptor subunit availability by microRNAs. J. Cell Biol. 185: 685–697.

Kim, G., and K. Kandler, 2010 Synaptic changes underlying the strengthening of GABA/glycinergic connections in the developing lateral superior olive. Neuroscience 171: 924–933.

Kinchen, J. M., and K. S. Ravichandran, 2010 Identification of two evolutionarily conserved genes regulating processing of engulfed apoptotic cells. Nature 464: 778–782.

Korkut, C., and V. Budnik, 2009 WNTs tune up the neuromuscular junction. Nat. Rev. Neurosci. 10: 627–634.

Korkut, C., Y. Li, K. Koles, C. Brewer, J. Ashley *et al.*, 2013 Regulation of postsynaptic retrograde signaling by presynaptic exosome release. Neuron 77: 1039–1046.

Lee, M. J., S. Jang, M. Nahm, J. H. Yoon, and S. Lee, 2013 Tbc1d15-17 regulates synaptic development at the *Drosophila* neuromuscular junction. Mol. Cells. 36: 163–168.

Lee, J., and C. F. Wu, 2010 Orchestration of stepwise synaptic growth by K+ and Ca2+ channels in Drosophila. J. Neurosci. 30: 15821–15833.

Littleton, J. T., and H. J. Bellen, 1995 Presynaptic proteins involved in exocytosis in Drosophila melanogaster: a genetic analysis. Invert. Neurosci. 1: 3–13.

Marrus, S. B., and A. DiAntonio, 2004 Preferential localization of glutamate receptors opposite sites of high presynaptic release. Curr. Biol. 14: 924–931.

Marrus, S. B., S. L. Portman, M. J. Allen, K. G. Moffat, and A. DiAntonio, 2004 Differential localization of glutamate receptor subunits at the Drosophila neuromuscular junction. J. Neurosci. 24: 1406–1415.

Mathew, S. J., S. Kerridge, and M. Leptin, 2009 A small genomic region containing several loci required for gastrulation in Drosophila. PLoS One 4: e7437.

Melom, J. E., Y. Akbergenova, J. P. Gavornik, and J. T. Littleton, 2013 Spontaneous and evoked release are independently regulated at individual active zones. J. Neurosci. 33: 17253–17263.

Menon, K. P., S. Sanyal, Y. Habara, R. Sanchez, R. P. Wharton *et al.*, 2004 The translational repressor Pumilio regulates presynaptic morphology and controls postsynaptic accumulation of translation factor eIF-4E. Neuron 44: 663–676.

Menon, K. P., S. Andrews, M. Murthy, E. R. Gavis, and K. Zinn, 2009 The translational repressors Nanos and Pumilio have divergent effects on presynaptic terminal growth and postsynaptic glutamate receptor subunit composition. J. Neurosci. 29: 5558–5572.

Nordmann, M., M. Cabrera, A. Perz, C. Brocker, C. Ostrowicz *et al.*, 2010 The Mon1-Ccz1 complex is the GEF of the late endosomal Rab7 homolog Ypt7. Curr. Biol. 20: 1654–1659.

Peled, E. S., Z. L. Newman, and E. Y. Isacoff, 2014 Evoked and spontaneous transmission favored by distinct sets of synapses. Curr. Biol. 24: 484–493.

Petersen, S. A., R. D. Fetter, J. N. Noordermeer, C. S. Goodman, and A. DiAntonio, 1997 Genetic analysis of glutamate receptors in Drosophila reveals a retrograde signal regulating presynaptic transmitter release. Neuron 19: 1237–1248.

Poteryaev, D., H. Fares, B. Bowerman, and A. Spang, 2007 Caenorhabditis elegans SAND-1 is essential for RAB-7 function in endosomal traffic. EMBO J. 26: 301–312.

Poteryaev, D., S. Datta, K. Ackema, M. Zerial, and A. Spang, 2010 Identification of the switch in early-to-late endosome transition. Cell 141: 497–508.

Raposo, G., and W. Stoorvogel, 2013 Extracellular vesicles: exosomes, microvesicles, and friends. J. Cell Biol. 200: 373–383.

Ratnaparkhi, A., G. M. Lawless, F. E. Schweizer, P. Golshani, and G. R. Jackson, 2008 A Drosophila model of ALS: human ALS-associated mutation in VAP33A suggests a dominant negative mechanism. PLoS One 3: e2334.

Sanyal, S., and M. Ramaswami, 2002 Spinsters, synaptic defects, and amaurotic idiocy. Neuron 36: 335–338.

Schmid, A., S. Hallermann, R. J. Kittel, O. Khorramshahi, A. M. Frolich *et al.*, 2008 Activity-dependent site-specific changes of glutamate receptor composition in vivo. Nat. Neurosci. 11: 659–666.

Sherwood, N. T., Q. Sun, M. Xue, B. Zhang, and K. Zinn, 2004 Drosophila spastin regulates synaptic microtubule networks and is required for normal motor function. PLoS Biol. 2: e429.

Shimizu, H., S. Kawamura, and K. Ozaki, 2003 An essential role of Rab5 in uniformity of synaptic vesicle size. J. Cell Sci. 116: 3583–3590.

Sigrist, S. J., P. R. Thiel, D. F. Reiff, P. E. Lachance, P. Lasko *et al.*, 2000 Postsynaptic translation affects the efficacy and morphology of neuromuscular junctions. Nature 405: 1062–1065.

Sigrist, S. J., P. R. Thiel, D. F. Reiff, and C. M. Schuster, 2002 The postsynaptic glutamate receptor subunit DGluR-IIA mediates long-term plasticity in Drosophila. J. Neurosci. 22: 7362–7372.

Sigrist, S. J., D. F. Reiff, P. R. Thiel, J. R. Steinert, and C. M. Schuster, 2003 Experience-dependent strengthening of Drosophila neuromuscular junctions. J. Neurosci. 23: 6546–6556.

Sudhof, T. C., 1995 The synaptic vesicle cycle: a cascade of protein-protein interactions. Nature 375: 645–653.

Sweeney, S. T., and G. W. Davis, 2002 Unrestricted synaptic growth in spinster-a late endosomal protein implicated in TGF-beta-mediated synaptic growth regulation. Neuron 36: 403–416.

Uytterhoeven, V., S. Kuenen, J. Kasprowicz, K. Miskiewicz, and P. Verstreken, 2011 Loss of skywalker reveals synaptic endosomes as sorting stations for synaptic vesicle proteins. Cell 145: 117–132.

Verhoeven, K., P. De Jonghe, K. Coen, N. Verpoorten, M. Auer-Grumbach *et al.*, 2003 Mutations in the small GTP-ase late endosomal protein RAB7 cause Charcot-Marie-Tooth type 2B neuropathy. Am. J. Hum. Genet. 72: 722–727.

Wagh, D. A., T. M. Rasse, E. Asan, A. Hofbauer, I. Schwenkert *et al.*, 2006 Bruchpilot, a protein with homology to ELKS/CAST, is required for structural integrity and function of synaptic active zones in Drosophila. Neuron 49: 833–844.

Wang, C. W., P. E. Stromhaug, J. Shima, and D. J. Klionsky, 2002 The Ccz1-Mon1 protein complex is required for the late step of multiple vacuole delivery pathways. J. Biol. Chem. 277: 47917–47927.

Wang, C. W., P. E. Stromhaug, E. J. Kauffman, L. S. Weisman, and D. J. Klionsky, 2003 Yeast homotypic vacuole fusion requires the Ccz1-Mon1 complex during the tethering/docking stage. J. Cell Biol. 163: 973–985.

Wucherpfennig, T., M. Wilsch-Brauninger, and M. Gonzalez-Gaitan, 2003 Role of Drosophila Rab5 during endosomal trafficking at the synapse and evoked neurotransmitter release. J. Cell Biol. 161: 609–624.

Yousefian, J., T. Troost, F. Grawe, T. Sasamura, M. Fortini *et al.*, 2013 Dmon1 controls recruitment of Rab7 to maturing endosomes in Drosophila. J. Cell Sci. 126: 1583–1594.

Zhong, P., W. Liu, Z. Gu, and Z. Yan, 2008 Serotonin facilitates long-term depression induction in prefrontal cortex via p38 MAPK/Rab5-mediated enhancement of AMPA receptor internalization. J. Physiol. 586: 4465–4479.

Communicating editor: I. Hariharan

GENETICS

Supporting Information
www.genetics.org/lookup/suppl/doi:10.1534/genetics.115.177402/-/DC1

A Presynaptic Regulatory System Acts Transsynaptically via Mon1 to Regulate Glutamate Receptor Levels in *Drosophila*

Senthilkumar Deivasigamani, Anagha Basargekar, Kumari Shweta, Pooja Sonavane, Girish S. Ratnaparkhi, and Anuradha Ratnaparkhi

DOI: 10.1534/genetics.115.177402

A pre-synaptic regulatory system acts trans-synaptically via Mon1 to regulate glutamate receptor levels in *Drosophila*.

Senthilkumar Deivasigamani [*,†], Anagha Basargekar[†,‡], Kumari Shweta[‡], Pooja Sonavane[‡,§], Girish S. Ratnaparkhi[*,**], Anuradha Ratnaparkhi[‡,††]

*Indian Institute of Science Education and Research (IISER), Homi Bhabha Road, Pashan, Pune 411 008 & [‡]Agharkar Research Institute, G.G. Agarkar Road, Pune 411 004

[††]Corresponding Author: Anuradha Ratnaparkhi, Agharkar Research Institute, G.G. Agarkar Road, Pune 411 004; anu.aripune@gmail.com

Figure S1

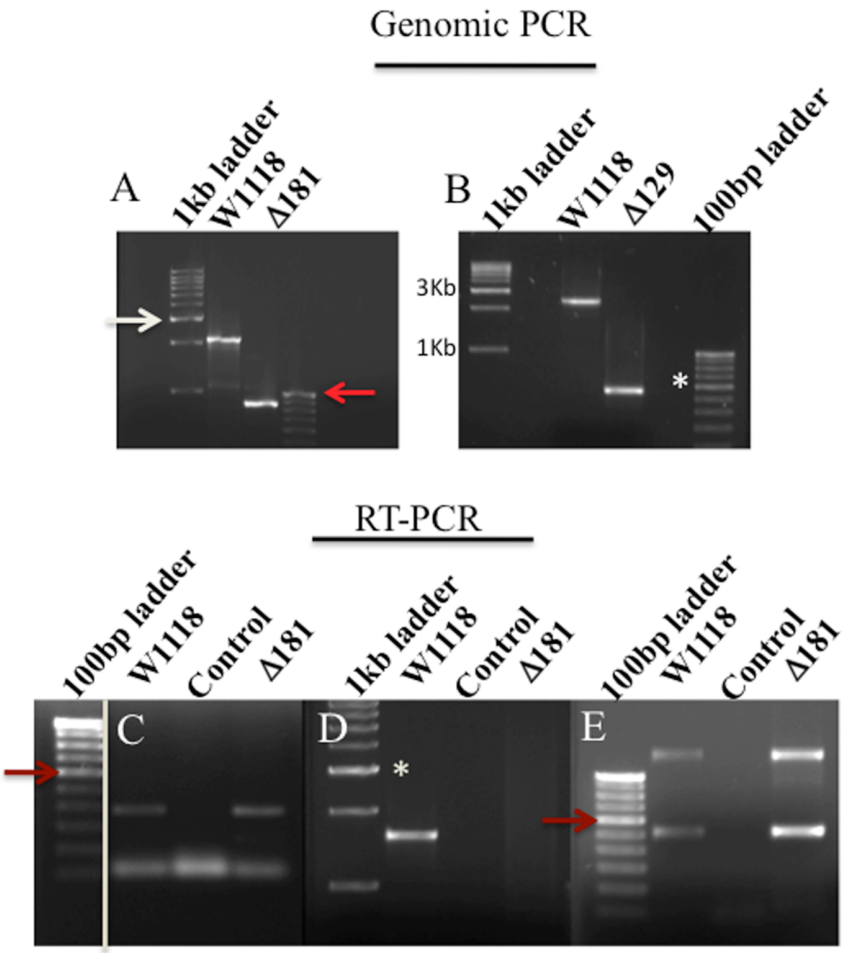

Figure S1: (A) Genomic PCR analysis of D181 mutants. Primers 2F and 31660_Ex2R (Fig1, gray arrows), amplify a 2128 base pair product with wildtype DNA. A band of approximately 850bp is seen with D181 DNA indicating a deletion between these primer sites. White arrow points to the 3kb band; the red arrow indicates 1kb.
(B) Genomic PCR analysis of D129 mutant. PCR with primers 3F and Int2_R2 (Fig1, red arrows) amplify a 2.4 kb region from wildtype DNA. In the D129 mutant, a smaller region of approximately 500bp is seen. The 600bp bright band (asterisk; 100bp ladder, Bangalore Genei, India) is spiked for easy identification.
(C-E) RT-PCR analysis of *Dmon1*$^{\Delta 181}$ mutants. (C) RT-PCR using primers 1F and 2R. The expected 340bp size band was amplified from cDNA derived from wildtype and *Dmon1*$^{\Delta 181}$ animals. The red arrow marks the 600bp band in the DNA ladder. The white line after the lane showing the DNA ladder and RT-PCR product denotes cropping of the lanes in the middle (D) PCR with primers 1F and 4R, amplified the full length *Dmon1*cDNA from wildtype but not *Dmon1*$^{\Delta 181}$ mutant indicating the absence of a full length transcript. The asterisk denotes a 3kb band. (E) PCR using primers designed to the 3' coding region of *CG31660/pog*. The two bands observed in each case correspond to different splice variants of *pog*. The red arrow marks the 600bp band. The middle lane in panels C,D and, and E is the no DNA RT-PCR control.

Figure S2

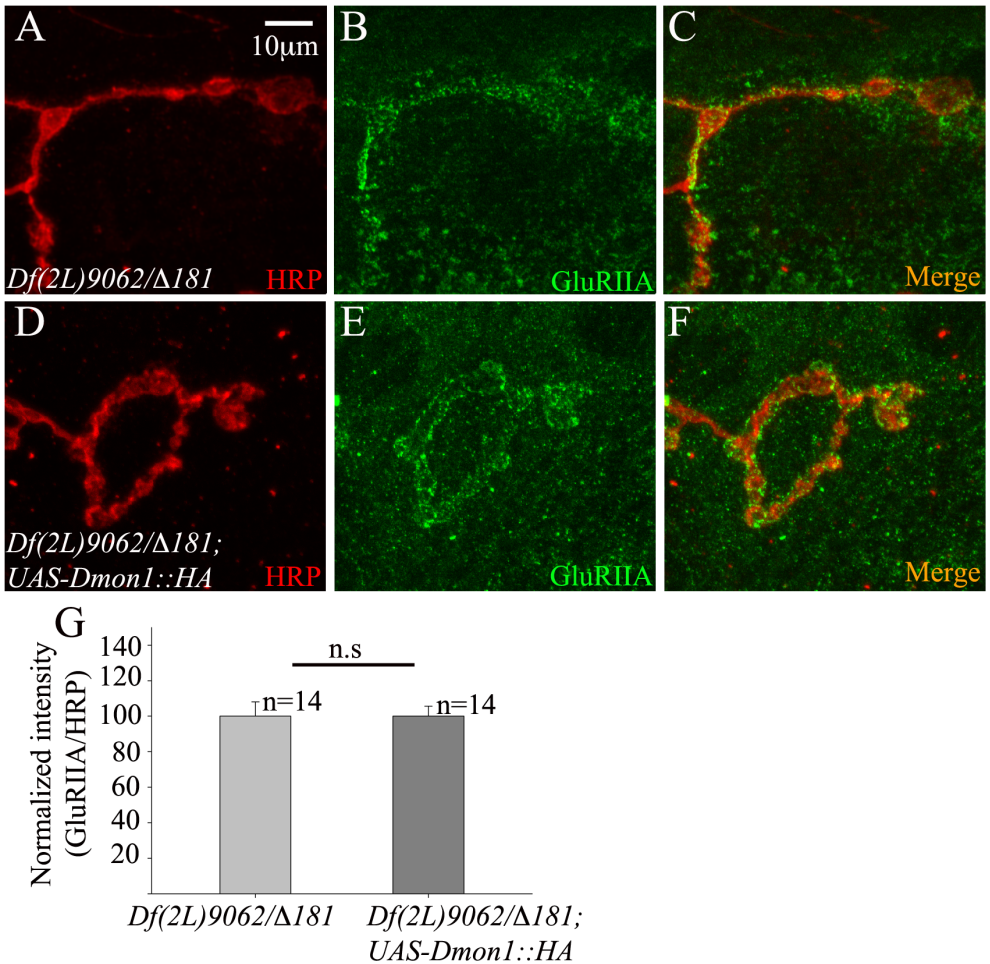

Figure S2. (A-C) Dmon1Δ181/Df(2L)9062 (D-F) Dmon1Δ181/Df(2L)9062; UAS-Dmon1::HA stained with anti-HRP (red) and anti-GluRIIA (green). (G). Normalized intensity (GluRIIA:HRP). No significant difference in intensity was observed between the two genotypes.

Figure S3

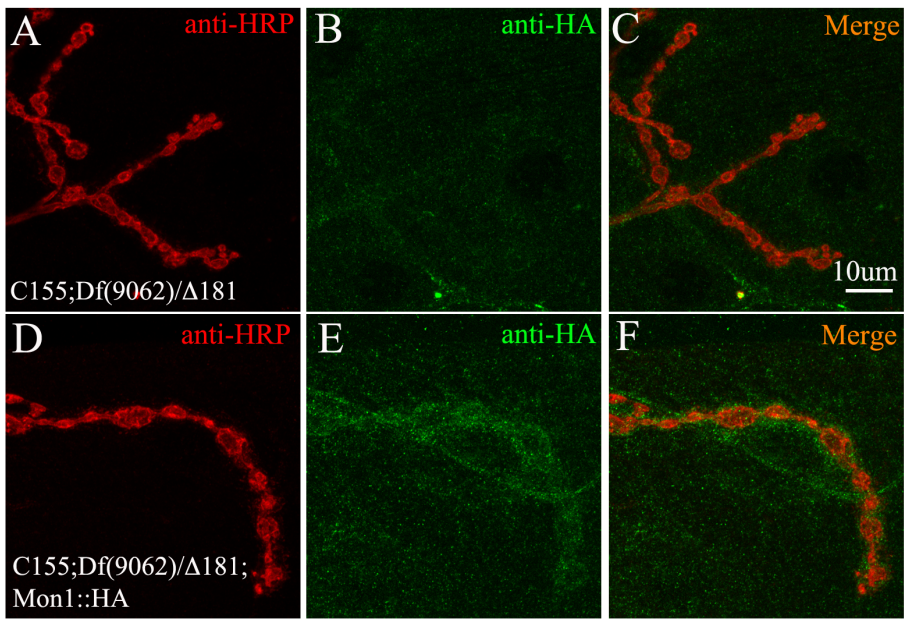

Figure S3. (A-C) Control (C155; Dmon1Δ181/Df(2L)9062) animals stained with anti-HRP (red) and anti-HA (green). (D-F) Expression of Dmon1::HA in a Dmon1 mutant background (C155; Dmon1Δ181/Df(2L)9062;UAS-Dmon1::HA). HA positive puncta are seen surrounding the bouton.